NASA TN D-362

TECHNICAL NOTE

D-362

EFFECTS OF TRANSIENT HEATING ON THE VIBRATION FREQUENCIES OF A PROTOTYPE OF THE X-15 WING

By Robert R. McWithey and Louis F. Vosteen

Langley Research Center
Langley Field, Va.

NATIONAL AERONAUTICS AND SPACE ADMINISTRATION

WASHINGTON

May 1960

NATIONAL AERONAUTICS AND SPACE ADMINISTRATION

TECHNICAL NOTE D-362

EFFECTS OF TRANSIENT HEATING ON THE VIBRATION FREQUENCIES OF A PROTOTYPE OF THE X-15 WING

By Robert R. McWithey and Louis F. Vosteen

SUMMARY

Radiant heating tests were conducted on a section of a prototype of the X-15 wing to determine the effect of aerodynamic heating on the effective stiffness of the wing. The aerodynamic-heating-rate distribution along the chord was obtained by means of radiant heaters positioned around the wing section which gave essentially identical heat inputs to the upper and lower surfaces. Changes in frequency of each of five natural modes of vibration of the wing section were determined to indicate changes in stiffness. The tests are described herein and the results discussed show that the largest change in frequency, a decrease of 5 percent, occurred in the first torsion mode. The change in effective stiffness was calculated for the first torsion mode by using the experimental temperature distribution and was found to be in fair agreement with the measured value.

INTRODUCTION

The high temperatures induced by aerodynamic heating may have adverse effects on the aeroelastic behavior of wing structures. Changes in stiffness due to changes in material properties are fairly well known and may be readily evaluated. Thermal stresses resulting from the nonlinear temperature distributions associated with aerodynamic heating may also have significant effects on wing stiffness. These effects were demonstrated by a theoretical calculation for the change in torsional stiffness of thin, solid wings subjected to aerodynamic heating as presented in reference 1. Reference 2 discusses supersonic jet tests of multiweb wings in which catastrophic flutter occurred because of aerodynamic heating. The problem of stiffness changes was investigated further in the tests reported in reference 3 in which changes in stiffness were determined by measuring changes in the frequencies of natural modes of vibration during transient heating.

As part of the development of the X-15 research airplane, it was desired to determine whether a proposed wing design was subject to

significant stiffness losses due to the transient heating imposed during flight. This report presents the effective stiffness changes obtained from transient-heating tests on a section of an early version of the X-15 wing. The aerodynamic-heating-rate distribution along the chord (as given by the predicted temperature-history curves for a reentry phase of a flight) was obtained by means of radiant heaters positioned around the wing. Changes in stiffness during the heating tests were found by measuring the changes in frequency of each of five natural modes of vibration of the wing section. A calculation of the change in effective stiffness for the first torsion mode (the mode which indicated the greatest stiffness change) is presented.

SYMBOLS

a,b	constants
f	frequency
l	length of model
r	radial distance from center of twist to point in cross section
s	length of skin between spars
t	skin thickness
x,y	rectangular coordinates
A	cross-sectional material area
E	Young's modulus
F	area of cell
G	shear modulus
I_p	mass polar moment of inertia of cross section
J	torsional stiffness constant
α	linear coefficient of thermal expansion
σ_y	normal stress
ΔT	temperature rise

Subscripts:

eff	effective
n	denotes nth cell
o	initial condition
t	elevated temperature conditions
B	bottom skin
T	top skin

TESTS

Model Description and Instrumentation

The model was an untapered multiweb-wing structure. The cross section of the model was identical to the cross section at the 75-percent-semispan station of a prototype X-15 wing. Figure 1 is a typical view of the cross section and plan form of the structure tested. The main structural box consisted of seven built-up titanium spars with 0.040-inch-thick spar caps and 0.020-inch-thick spar webs, two 0.063-inch-thick formed titanium spars, 0.060-inch-thick Inconel X skins, and 0.050-inch-thick ribs at the root and tip. The leading-edge portion of the structure consisted of 0.125-inch-thick Inconel X leading-edge skin attached to a 0.050-inch-thick formed titanium spar just back of the leading edge, and 0.063-inch-thick Inconel X skins between the spar and the main structural box. Five equally spaced formed channel ribs 0.040 inch thick were also located between the leading-edge spar and the main structural box.

The model was mounted as a cantilever by means of heavy reinforced angles bolted to the skins of the main structural box at the root. Slots were cut diagonally in the main skins at the root and tip as shown in figure 1 to alleviate thermal stresses. It should be noted that the leading-edge portion of the structure was not attached to the mounting angles.

Thermocouples were installed along the chord and span at the points indicated in figure 2. An auxiliary thermocouple was installed adjacent to each thermocouple position indicated in figure 2 and was used in the event the original thermocouple failed.

Apparatus and Test Procedure

A general view of the test area is shown in figure 3. A closeup view of the model is shown in figure 4. The model was mounted horizontally as a cantilever and vibrated by means of two 10-pound maximum-force electromagnetic shakers. The electrical connections to the two shakers were such that the exciting forces could be supplied to the structure either in phase or 180° out of phase with each shaker supplying an equal force to the model. Shaker connecting rods were attached to the model at the tip near the leading-edge spar and trailing-edge spar of the main structural box as shown in figure 4. A frequency survey of the model from 16 cycles per second to 205 cycles per second was made before heating.

During the heating tests, the wing was vibrated at the resonant frequency using the resonance-following system described in reference 3. Briefly, the resonance-following system is a servo system which maintains a constant phase relation between the applied force, as indicated by a signal generator, and response of the model, as indicated by a vibration pickup on the model.

The model response was determined by using a strain-gage beam as the vibration pickup. One end of the beam was clamped to the tip of the model and the other end clamped to a fixed support. The beam length, width, and thickness were 3 inches, 3/8 inch, and 0.020 inch, respectively. Two SR-4 strain gages, type CB-7, were attached to each side of the beam near the fixed support and were connected in a four-active-arm bridge. Bridge voltage was supplied by two 45-volt batteries in parallel. The bridge output was connected directly to the phase detector of the resonance-following system.

In order to obtain a history of the model frequency during a heating test, a position indicator was geared to the frequency-adjustment shaft of the signal generator and calibrated to indicate the shaker frequency. The frequency was recorded continuously during the tests. The error in the ability of the resonance-following system to maintain resonance is less than 1 percent of the resonant frequency.

In order to obtain the maximum temperature rise rates required, three heaters were arranged as shown in figure 4. The upper and lower surfaces of the wing received essentially identical heat inputs. The desired model heating-rate distribution was determined from the linear portion of the predicted temperature-history curves for the bottom skin for a reentry phase of the X-15 flight program. This portion of the predicted curves could be easily reproduced by the radiant heating apparatus used in these tests. The maximum heating-rate distribution obtained along the instrumented chord line and the maximum heating rate desired are shown in figure 5. The leading-edge heater was operated at

an average power density of 400 watts per square inch and the other heaters at an average power density of 64 watts per square inch. All heaters were energized simultaneously at the beginning of each test. After approximately 40 seconds, the temperature of the leading edge reached 1,250° F. At this time the power to the front heater was interrupted and supplied intermittently as required to keep the temperature of the leading edge at 1,250° F for the remainder of the test. The maximum skin temperature desired was obtained experimentally in a total heating time of 2 minutes, approximately the same time as that given by the expected-flight-temperature curves. Temperatures were recorded continuously during the tests.

RESULTS AND DISCUSSION

The frequency survey of the model from 16 cycles per second to 205 cycles per second, made before heating, disclosed seven natural modes in this range. The nodal line patterns and frequencies for these seven modes are shown in figure 6. The effect of heating on five of the modes (designated A, B, D, F, and G) was found; the other two modes (C and E) yielded resonance peaks which were too weak to operate the resonance-following system. The modes investigated were first bending (mode A), first torsion (mode B), and three modes (modes D, F, and G) involving considerable amounts of chordwise bending. Figure 6 also shows the frequency history during heating for each mode investigated. The ordinate scale is the ratio of model frequency f to initial mode frequency f_o. Changes in the natural frequency indicate small changes in stiffness throughout the test for all the modes investigated. Modes A, B, and G indicated a decrease in structural stiffness. Mode D indicated an increase in structural stiffness, whereas mode F indicated little change. The largest change in stiffness appeared in the first torsion mode (mode B) where the frequency decreased 5 percent. The results of a frequency survey, which was made after the completion of the heating tests, were compared with the results of the initial frequency survey and showed no change in the resonance characteristics of the model.

During the initial heating portion of each test (before the leading edge reached 1,250° F), an inward buckle gradually appeared between each rib in the upper leading-edge skin between the leading-edge spar and the main structural box. No appreciable change in buckle pattern or depth of the buckle was noted after the initial heating portion of each test. After the first few tests some permanent deformation could be seen in the leading-edge skin, but the deformation did not increase in subsequent tests. The lower skin between the leading-edge spar and main structural box did not appear to buckle during the tests although it deformed at the tip.

Inasmuch as only 34 recording channels were used to record temperature data, all thermocouples could not be recorded on each test. Tables 1, 2, and 3 give temperature data obtained from each of three typical tests and indicate the temperature change for each thermocouple location shown in figure 2. Included in table 3 are data taken during a test in which the auxiliary thermocouples at positions 5, 21, 30, and 34 were used inasmuch as the regular thermocouples at the positions gave unreliable readings. The accuracy of the temperature readings is within $\pm 8^{\circ}$ F.

The temperature distribution along the instrumented chord line after 120 seconds of heating is shown in figure 7. The indicated temperatures were obtained from the three tests for which the data are given in tables 1, 2, and 3. It may be noted from the tables that the recorded temperatures were duplicated within 10 percent from test to test.

The curve shown in figure 7 is a faired line through the recorded skin temperatures. The temperature distribution along the instrumented span line is fairly uniform and may be determined from the data of table 2 for thermocouples 32, 33, 35, 36, and 37. The spar at the trailing edge received radiation from the heaters which accounts for the higher spar-web temperature indicated by thermocouple 51.

CALCULATION OF STIFFNESS CHANGE FOR FIRST TORSION MODE AND COMPARISON WITH TEST RESULTS

The test results indicate that the greatest change in frequency for the first torsion mode occurred at the end of the test. Therefore the following calculations concerning the change in stiffness are based upon the temperature distribution present in the structure at 120 seconds.

An equation relating the change in torsional stiffness of a thin wing to axial thermal stress is given in reference 1 as

$$\frac{(GJ)_{eff}}{(GJ)_o} = 1 + \frac{\int_A \sigma_y r^2 dA}{(GJ)_o} \qquad (1)$$

where σ_y is the spanwise normal stress and r is the radial distance from the center of twist. In order to include the effect of temperature upon the shear modulus of the skin, equation (1) may be written as

$$\frac{(GJ)_{eff}}{(GJ)_o} = \frac{G_t}{G_o} + \frac{\int_A \sigma_y r^2 dA}{(GJ)_o} \tag{2}$$

where G_t is the shear modulus of the skin material at a given temperature and G_o is the shear modulus of the skin material at room temperature.

In order to determine the value of $\int_A \sigma_y r^2 dA$, the cross section was divided into 53 elements with the relative size of each element dependent upon the magnitude of the temperature gradient. For a free-end beam, the value of the integral will be independent of the axis of twist and therefore, for simplicity, the reference axes were taken at the leading edge as shown in the following sketch.

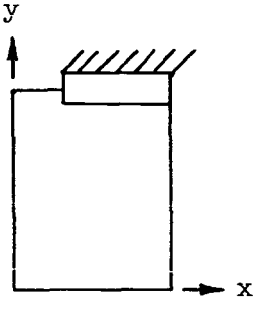

If the plane sections remain plane, the axial thermal stress σ_y may be determined from the equation

$$\sigma_y = E(a + bx - \alpha \Delta T) \tag{3}$$

where ΔT is the temperature change for an element of the cross section and a and b are constants determined from the equilibrium conditions of zero net thrust and net moment. The value of Young's modulus was based on the average temperature of each element. The radial distance r was taken as the distance along the x-axis inasmuch as the model is thin. Integrating $\sigma_y r^2 dA$ numerically over the cross section gives

$$\int_A \sigma_y r^2 dA = -9.7 \times 10^6 \text{ lb-in.}^2 \tag{4}$$

The value of G_t is based upon the average skin temperature (770° F) present at 120 seconds. The ratio of G_t to G_o for this condition is (from ref. 4)

$$\frac{G_t}{G_o} = 0.88 \tag{5}$$

In order to determine the relative magnitude of the stiffness change, the value of $(GJ)_o$ must be determined. Because of the complexity of the structure and the manner in which it was mounted, an accurate theoretical determination of $(GJ)_o$ is very difficult.

An upper limit for the value of J for a multicell structure is given by equation 2.22 of reference 5 as

$$J = 4 \sum^{n} \frac{F_n^2}{\frac{s_{nT}}{t_{nT}} + \frac{s_{nB}}{t_{nB}}} \tag{6}$$

where F_n is the area of the nth cell and s_{nT}, t_{nT}, s_{nB}, and t_{nB} denote the width of the skin between spars and skin thickness for the upper and lower skins, respectively, for the nth cell. The value of the initial torsional stiffness constant $(GJ)_o$ for the structural box was calculated to be 192×10^6 lb-in^2. In order to calculate the frequency of the first torsion mode, the above value of $(GJ)_o$ was used and the end support was assumed to be perfectly rigid. The frequency, in cycles per second, is then given by

$$f = \frac{1}{4l}\sqrt{\frac{GJ}{I_p}} \tag{7}$$

where l is the length of the model and I_p was taken as the mass polar moment of inertia of the cross section about the center of gravity. The frequency of the first torsion mode found from equation (7) is 94 cycles per second. The difference between calculated and measured frequencies may be attributed to the flexible end support, the fact that the mode was not pure torsion, and errors in the assumption for the calculation of the torsional stiffness.

It should be noted that the first term on the right-hand side of equation (2) denotes a 12-percent reduction in stiffness due to changes in material properties; whereas, the reduction in stiffness due to thermal stresses, as indicated by the second term, is approximately 5 percent.

The ratio of the wing frequency to the initial frequency of the first torsion mode was calculated to be 0.911. Note that the frequency ratio is proportional to the square root of the torsional stiffness ratio. As shown in figure 6, the measured frequency ratio was 0.948. Thus the reduction in frequency ratio obtained from the test is of the same order of magnitude as that obtained from the calculation.

CONCLUDING REMARKS

Frequency changes for five natural modes of vibration of a version of the X-15 wing were measured during simulated aerodynamic heating to determine any changes in stiffness. No large changes in stiffness occurred for the modes investigated. The largest stiffness change was found during the test of the first torsion mode in which a frequency decrease of 5 percent was measured. A calculation for the torsional stiffness change based upon the experimental temperature distribution present at the end of the test was in fair agreement with the measured change.

Langley Research Center,
National Aeronautics and Space Administration,
Langley Field, Va., January 15, 1960.

REFERENCES

1. Budiansky, Bernard, and Mayers, J.: Influence of Aerodynamic Heating on the Effective Torsional Stiffness of Thin Wings. Jour. Aero. Sci., vol. 23, no. 12, Dec. 1956, pp. 1081-1093, 1108.

2. Heldenfels, Richard R., and Rosecrans, Richard: Preliminary Results of Supersonic-Jet Tests of Simplified Wing Structures. NACA RM L53E26a, 1953.

3. Vosteen, Louis F., McWithey, Robert R., and Thomson, Robert G.: Effect of Transient Heating on Vibration Frequencies of Some Simple Wing Structures. NACA TN 4054, 1957.

4. Kurg, Ivo M.: Tensile Properties of Inconel X Sheet Under Rapid-Heating and Constant-Temperature Conditions. NACA TN 4065, 1957.

5. Kuhn, Paul: Stresses in Aircraft and Shell Structures. McGraw-Hill Book Co., Inc., 1956.

TABLE 1

TEMPERATURE RISE OF MODEL

Thermocouple	Temperature rise °F for -									
	0, sec	10.0, sec	20.0, sec	30.0, sec	40.0, sec	40.2,* sec	60.0, sec	80.0, sec	100.0, sec	120.0, sec
1	0	416	771	1,029	1,230	1,239	1,248	1,243	1,256	1,261
2	0	91	196	301	405	407	549	675	784	871
3	0	88	184	285	398	398	547	683	788	867
4	0	70	145	224	294	298	386	461	531	606
8	0	99	211	309	404	408	533	636	713	782
9	0	92	210	302	394	398	525	625	700	765
10	0	4	22	48	92	96	192	305	406	510
11	0	77	189	263	340	340	456	534	603	672
12	0	13	51	89	132	132	209	285	349	418
13	0	18	58	94	130	130	206	278	331	398
14	0	0	22	31	39	39	83	153	215	289
15	0	96	212	304	396	396	516	612	679	750
18	0	81	188	269	350	350	471	565	632	699
19	0	81	193	265	341	341	453	543	602	664
20	0	80	172	256	331	335	446	543	618	689
22	0	70	140	206	263	268	360	448	522	588
23	0	17	64	120	184	185	291	382	459	536
24	0	17	65	113	174	174	253	340	410	484
25	0	4	4	13	35	39	118	170	244	322
26	0	0	5	23	42	46	102	171	241	319
27	0	9	9	9	22	22	70	135	200	287
28	0	78	156	225	285	285	376	467	532	601
31	0	9	9	17	35	35	86	147	229	311
38	0	0	9	17	39	39	91	153	240	322
39	0	87	165	248	326	326	439	521	617	682
40	0	61	138	212	277	277	372	458	540	609
41	0	0	4	13	30	30	78	134	207	290
42	0	17	70	127	188	188	288	371	458	537
43	0	80	160	235	306	311	422	511	599	662
44	0	69	143	208	273	278	377	469	555	616
45	0	0	4	4	18	18	65	126	201	275
46	0	31	110	193	268	268	373	470	557	627
47	0	66	136	189	259	259	360	452	540	611
48	0	0	4	6	18	18	62	119	190	268

*Leading-edge heater intermittent after this time.

TABLE 2

TEMPERATURE RISE OF MODEL

Thermocouple	Temperature rise °F for -									
	0, sec	10.0, sec	20.0, sec	30.0, sec	33.3,* sec	40.0, sec	60.0, sec	80.0, sec	100.0, sec	120.0, sec
1	0	463	833	1,111	1,190	1,186	1,190	1,204	1,217	1,230
2	0	100	213	318	357	405	536	657	749	827
3	0	92	201	305	349	401	536	667	754	833
4	0	74	157	235	261	292	374	448	509	579
6	0	119	242	347	387	431	549	655	725	800
7	0	112	220	311	350	380	475	565	626	699
8	0	102	204	298	338	373	489	596	667	742
9	0	109	222	317	357	398	516	629	701	782
11	0	72	175	260	277	324	422	511	588	656
14	0	0	13	17	25	38	79	138	213	276
15	0	91	186	277	308	347	459	542	624	693
16	0	86	186	290	307	363	476	557	649	709
17	0	0	13	23	32	41	96	160	234	316
18	0	87	179	275	297	345	445	542	642	703
19	0	86	177	276	293	345	452	530	620	685
20	0	97	186	274	291	342	452	540	625	696
27	0	0	13	17	25	38	80	147	219	295
29	0	85	178	276	294	347	454	530	624	686
32	0	70	145	223	240	281	380	454	533	591
35	0	84	180	260	302	331	449	562	637	717
36	0	86	181	271	301	340	460	559	645	722
37	0	82	159	236	262	296	395	480	553	609
39	0	87	173	260	281	329	433	528	606	675
40	0	73	281	225	255	285	389	475	553	622
43	0	81	158	239	268	302	409	498	579	652
44	0	77	154	227	262	292	399	480	562	631
46	0	80	164	244	279	310	421	518	602	673
47	0	68	136	204	236	264	364	452	528	604
49	0	77	158	240	270	304	415	509	591	668
50	0	68	131	199	233	259	356	445	522	602
51	0	0	22	31	39	57	113	187	266	336
52	0	56	129	185	198	233	315	392	470	534
53	0	65	138	186	194	233	350	380	449	510

*Leading-edge heater intermittent after this time.

TABLE 3

TEMPERATURE RISE OF MODEL

[The primary and auxiliary thermocouples at position 34 were defective; hence no data are tabulated for this position]

Thermocouple	Temperature rise °F for -									
	0, sec	10.0, sec	20.0, sec	30.0, sec	34.0,* sec	40.0, sec	60.0, sec	80.0, sec	100.0, sec	120.0, sec
1	0	437	789	1,044	1,140	1,124	1,162	1,130	1,146	1,151
2	0	85	202	298	351	378	521	628	713	782
4	0	59	144	208	245	261	346	410	474	533
5**	0	0	5	27	43	64	155	251	337	417
6	0	97	209	306	354	386	509	600	690	740
7	0	85	197	272	325	347	448	522	581	650
8	0	102	210	301	349	376	500	602	677	747
19	0	86	172	253	280	328	420	506	533	646
20	0	93	175	263	290	329	427	509	602	657
21**	0	75	150	231	253	290	376	462	554	613
22	0	82	152	229	245	278	359	424	517	588
24	0	32	86	134	139	177	252	327	412	471
25	0	11	22	38	43	54	97	162	248	318
27	0	5	5	27	32	43	75	129	210	280
29	0	90	181	276	298	340	441	516	611	675
30**	0	64	161	230	268	294	396	482	557	626
33	0	101	176	277	304	347	453	538	640	698

*Leading-edge heater intermittent after this time.

**Readings obtained from auxiliary thermocouples.

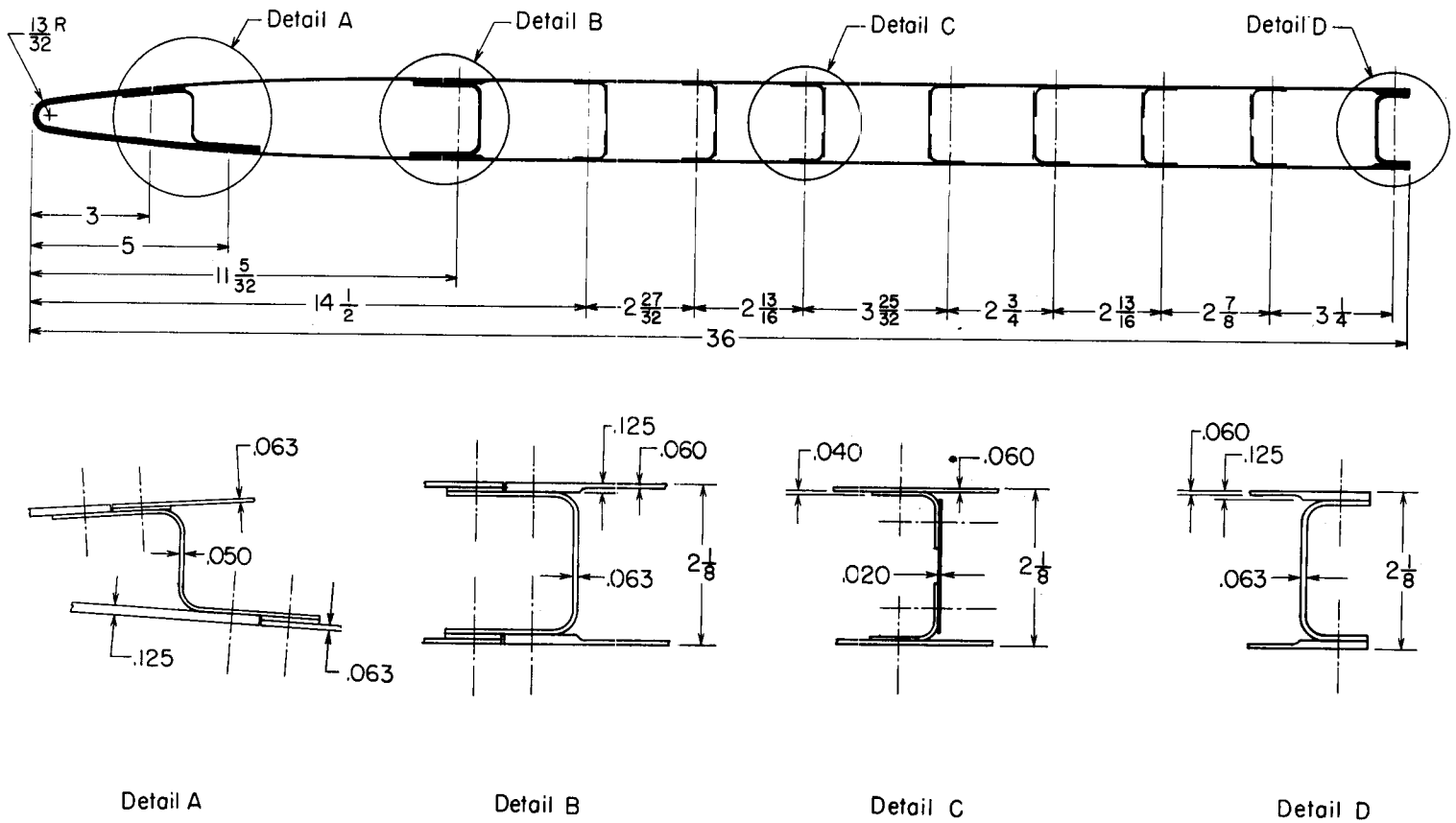

(a) View of cross section.

Figure 1.- Structural details of multiweb structure.

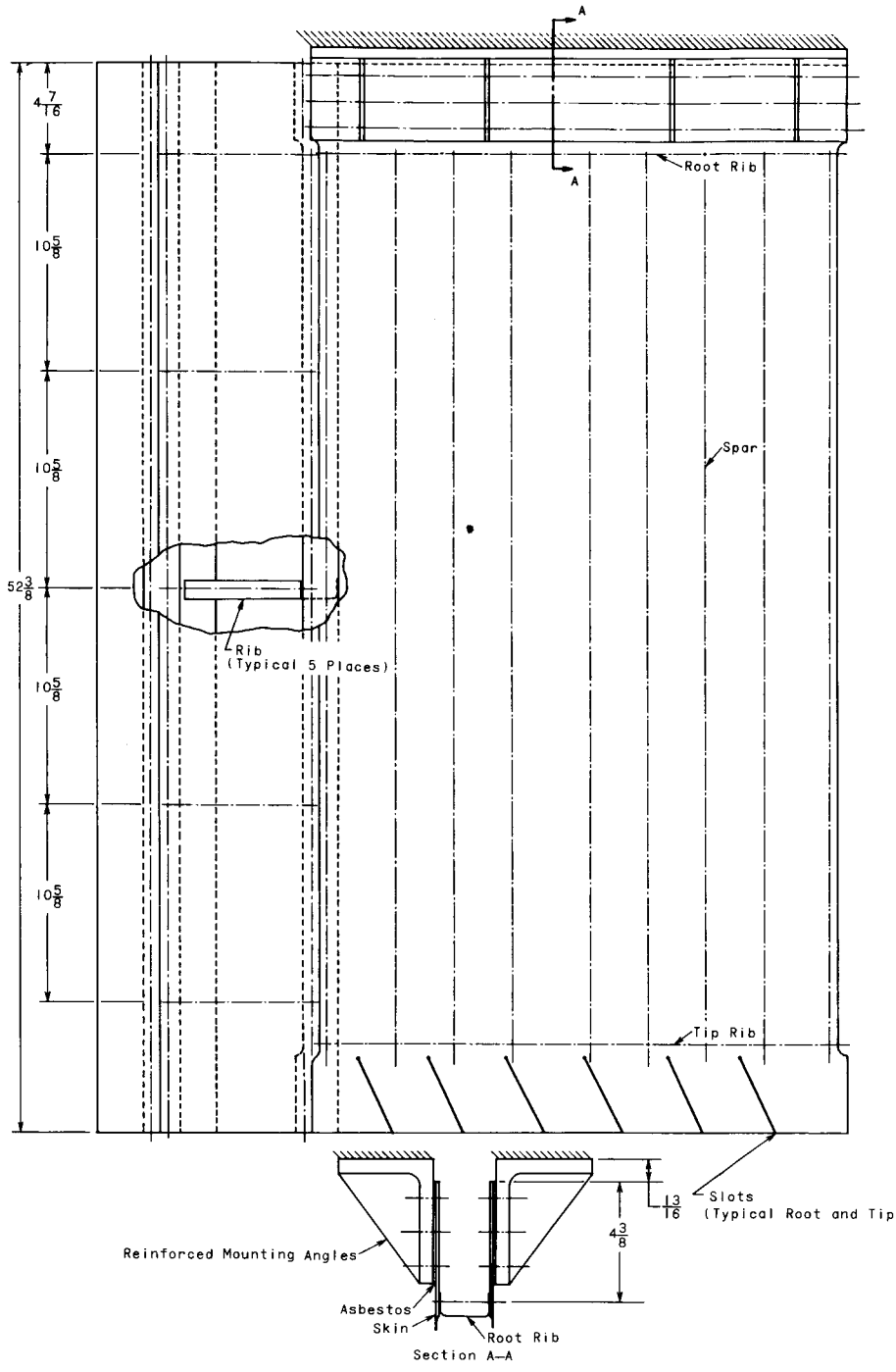

(b) View of plan form.

Figure 1.- Concluded.

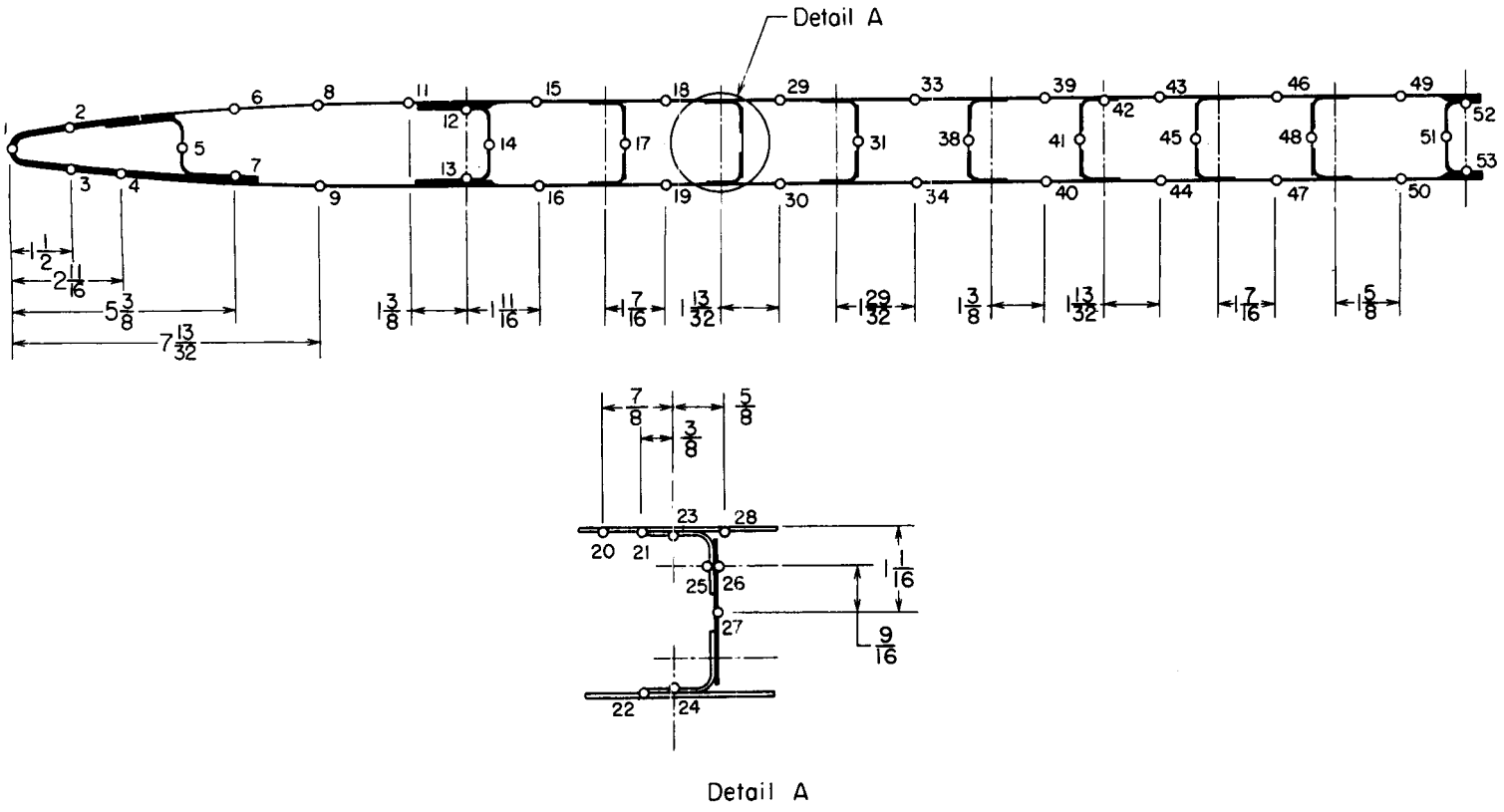

(a) Chord-line instrumentation.

Figure 2.- Thermocouple location. Circles denote thermocouple location.

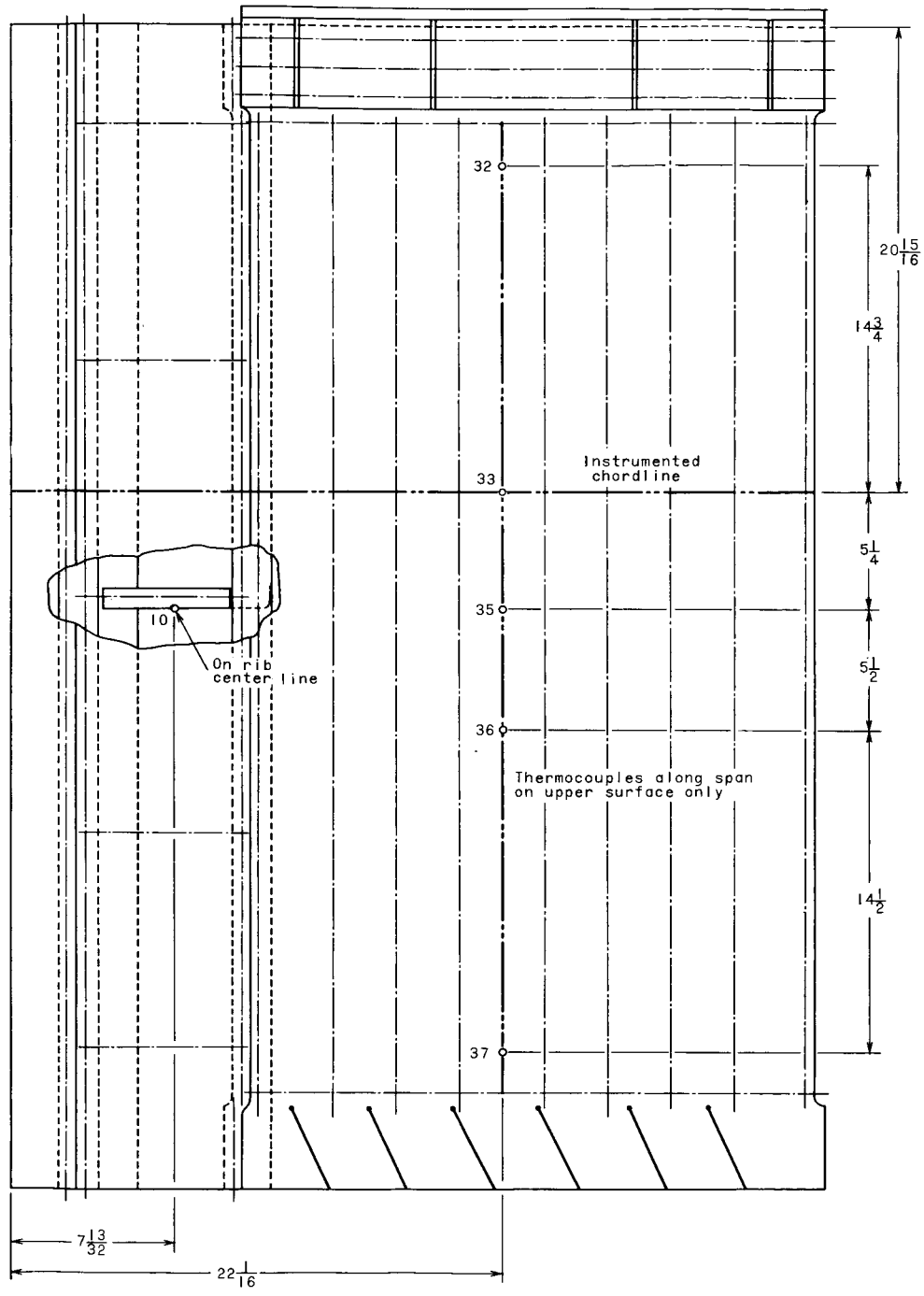

(b) Plan-form instrumentation.

Figure 2.- Concluded.

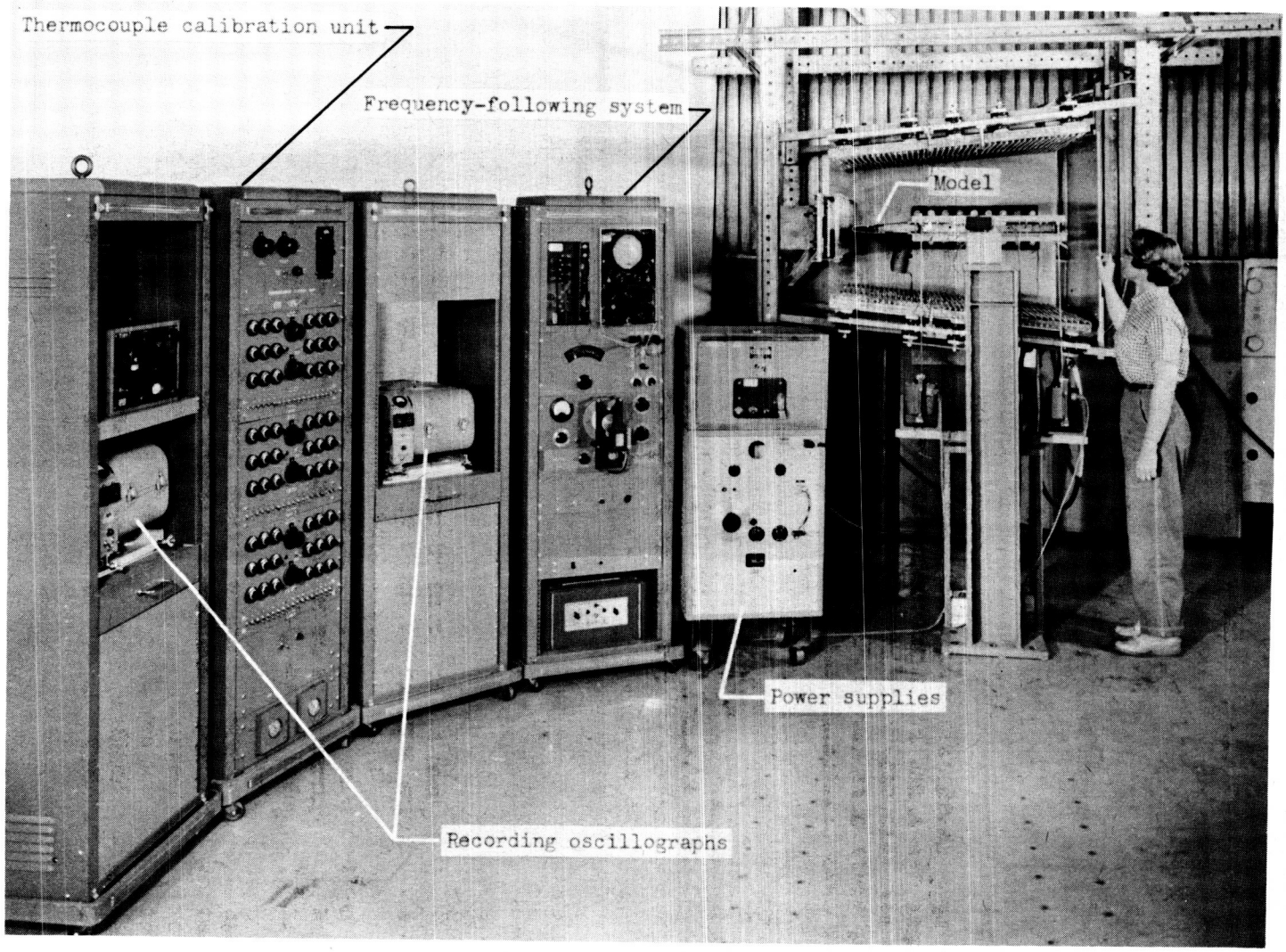

Figure 3.- View of test area and test apparatus. L-57-1889.2

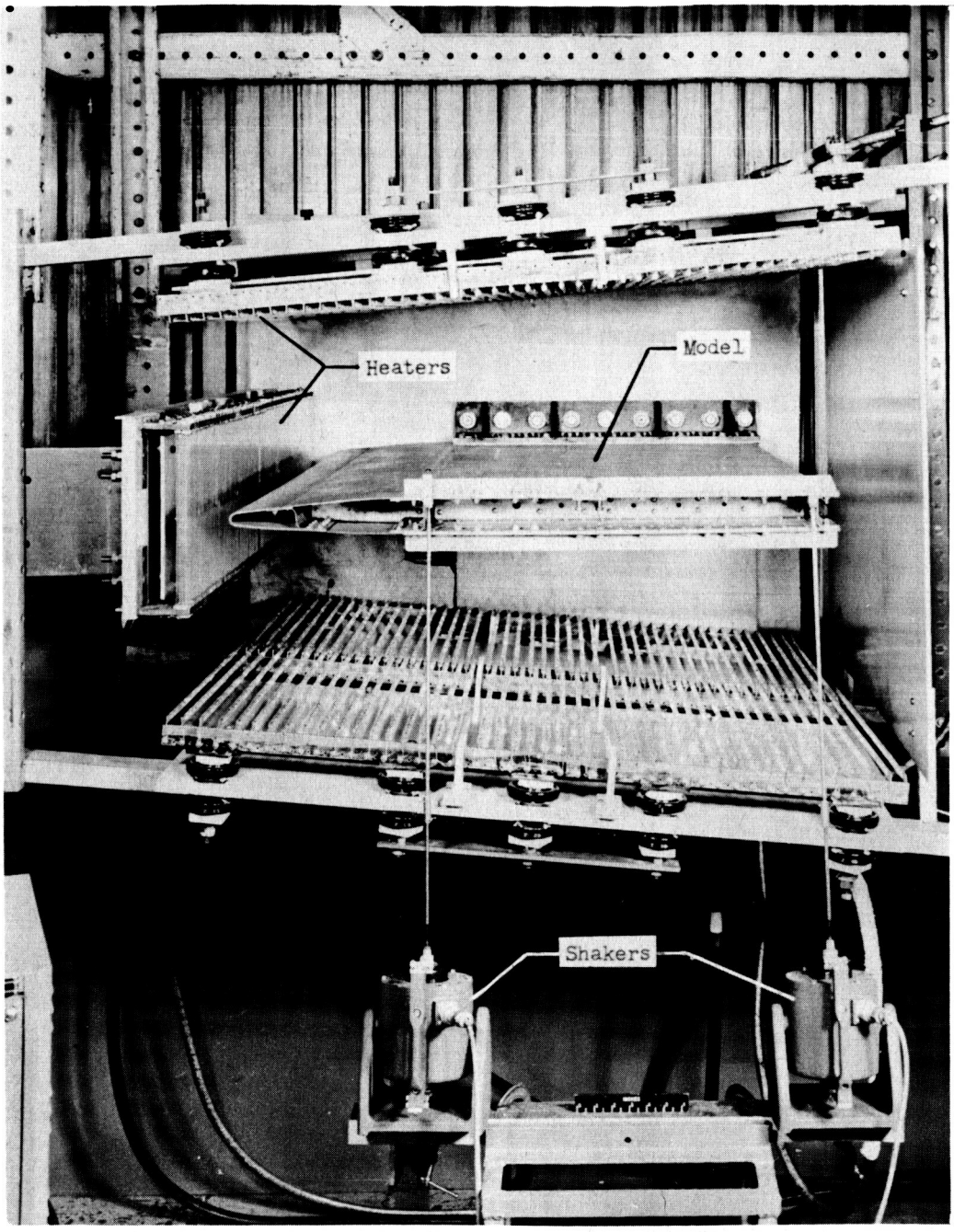

L-57-1891.1

Figure 4.- Closeup of test setup showing the location of the model, electromagnetic shakers, and radiant heaters.

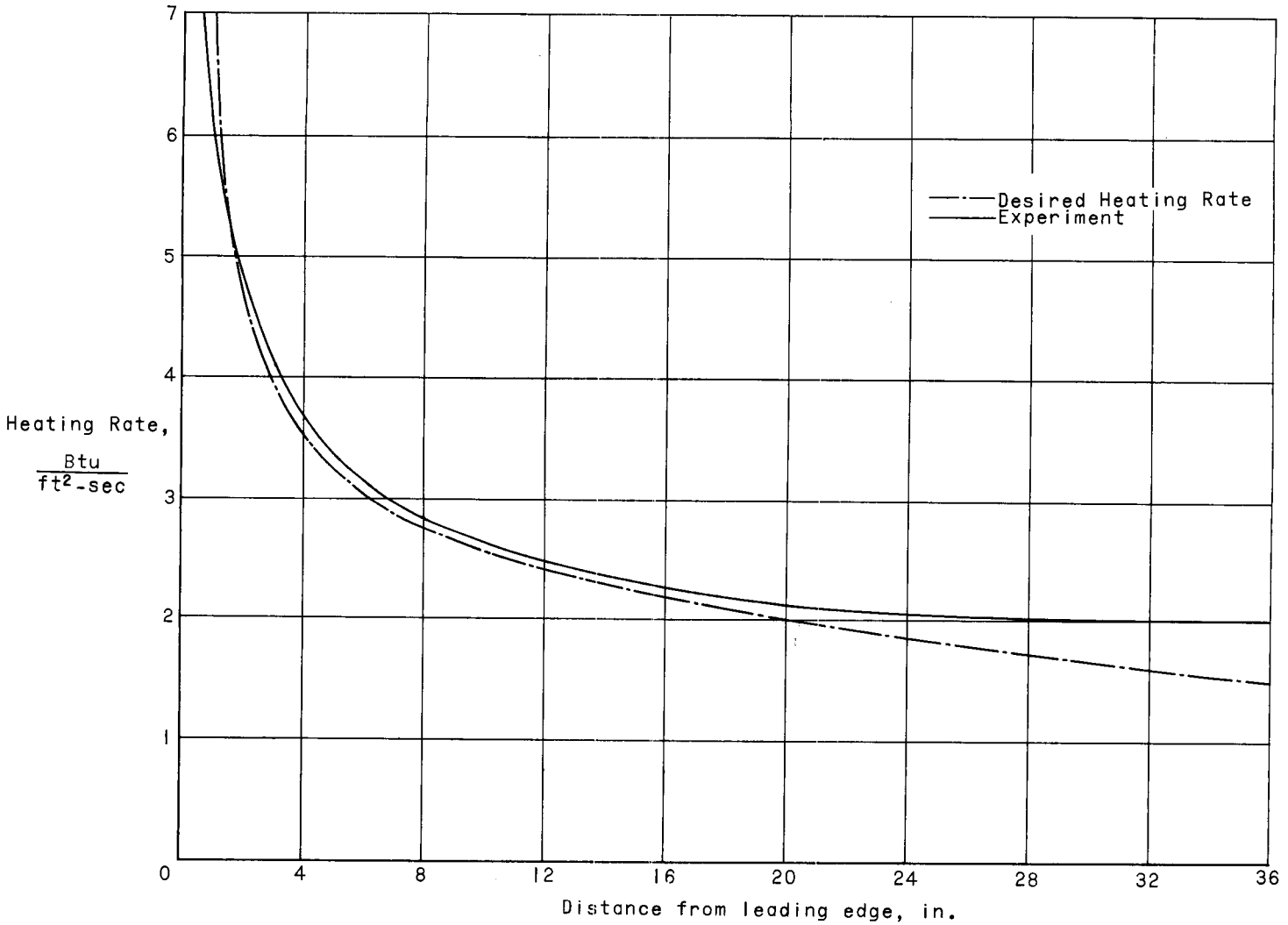

Figure 5.- Maximum heating-rate distribution along instrumented chord line. Experimental curve is initial heating-rate distribution.

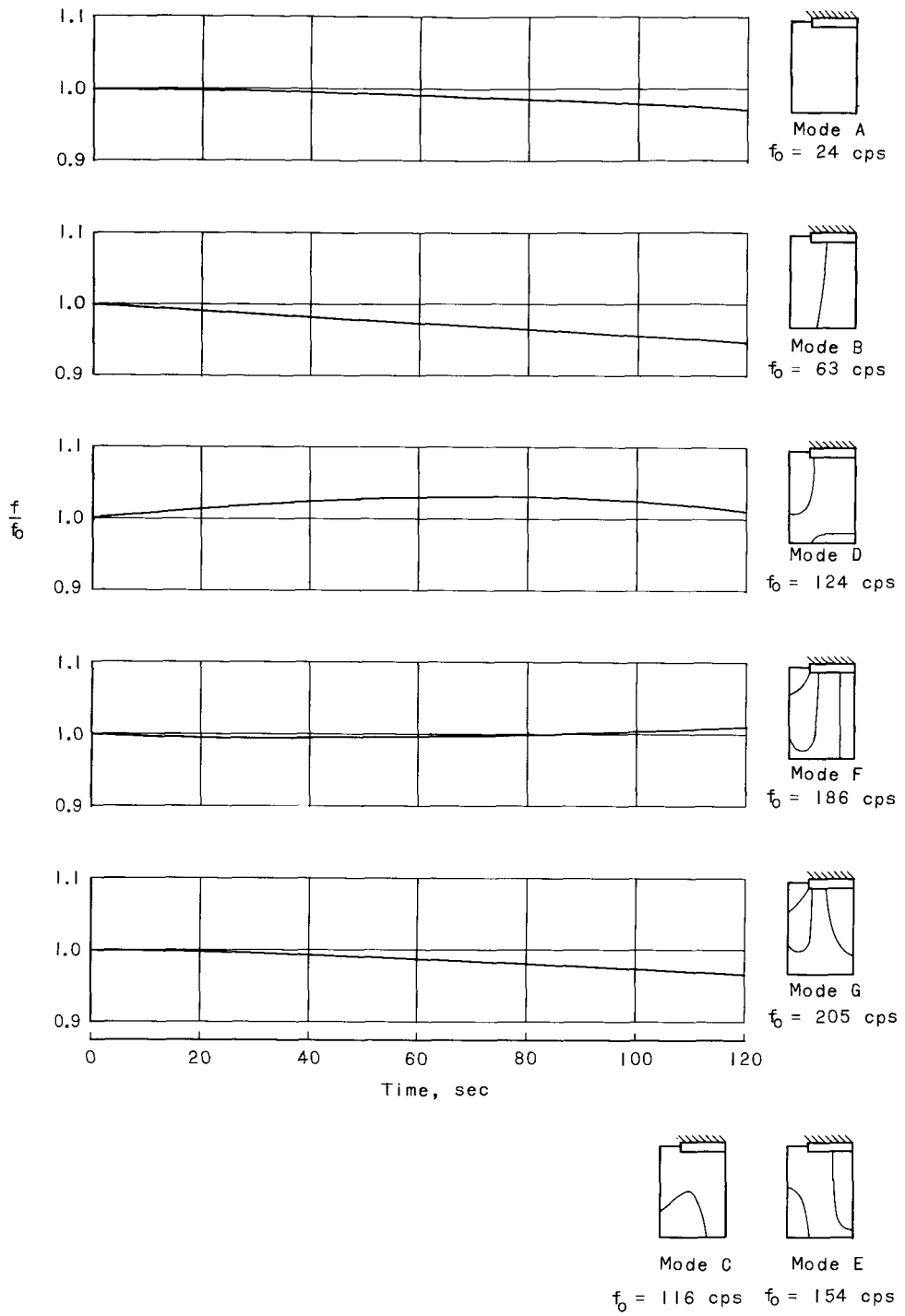

Figure 6.- Vibration-frequency histories and initial nodal patterns. No vibration-frequency histories were obtained for modes C and E.

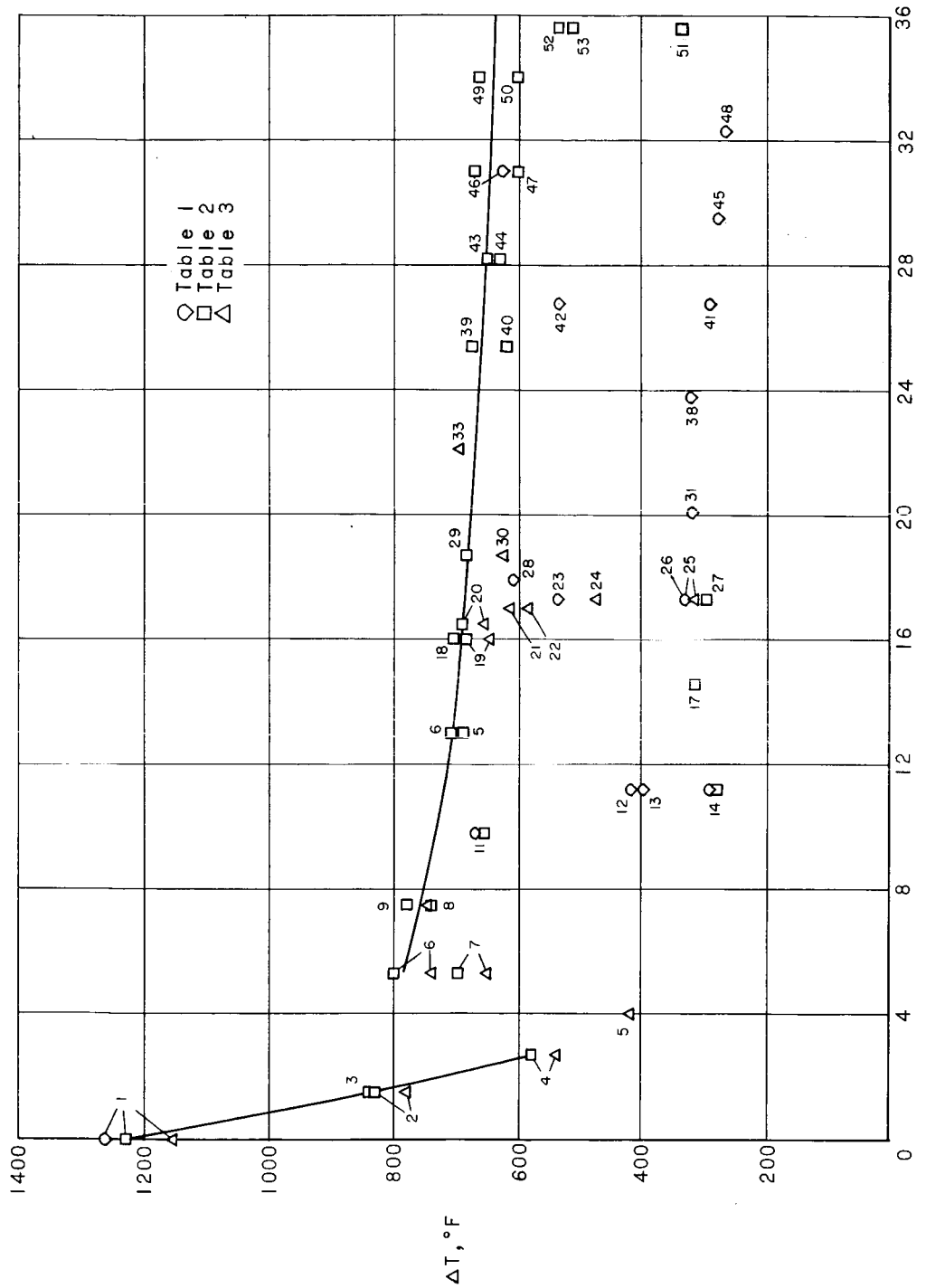

Figure 7.- Chordwise temperature distribution after 120 seconds of heating. The curve is a faired line through the maximum skin temperatures.